metals

MDPI

Article

Effects of Melting/Casting and Thermal Treatment Surrounding Gas Phase Composition on the Properties of a Low-Alloyed Steel

Guillaume Ah-lung [1,†], Ayyoube Barchid [1,†], Brahim Boubeker [1], Youssef Samih [1], Jones Alami [1], Sanae Baki Senhaji [2] and Johan Jacquemin [1,*]

[1] Materials Science and Nano-Engineering (MSN) Department, Accelerated Research Center for Metallurgy (ARC Metallurgy–MSN Site), Mohammed VI Polytechnic University (UM6P), Lot 660-Hay Moulay Rachid, Benguerir 43150, Morocco
[2] Maghreb Steel, Accelerated Research Center for Metallurgy (ARC Metallurgy–Maghreb Steel Site), Route Nationale 9, km 10, Casablanca 20600, Morocco
* Correspondence: johan.jacquemin@um6p.ma; Tel.: +212-666-933-996
† These authors contribute equally to this work.

Abstract: This study aims to provide insights into the experimental conditions used during the melting/casting process and subsequent thermal treatments of low-alloy steels, particularly regarding recycled scrap metals. As sustainable practices in metallurgy gain importance, optimizing scrap metal recycling is crucial for producing steel grades with desired chemical compositions, microstructures, and physical properties. Understanding these conditions is vital for enhancing the efficiency and quality of steel production from recycled materials. This study emphasizes the critical role of specific experimental conditions in the steelmaking process, especially with recycled scrap metals. It closely examines the atmosphere during melting/casting to identify key parameters that must be rigorously controlled in lab-scale steel production using a vacuum induction furnace. The findings indicate that both the chemical composition and recyclability of low-alloyed steels are significantly influenced by the surrounding atmosphere during melting and casting. Inert environments, such as vacuum or argon, are shown to be ideal for steelmaking with induction technology, particularly when recycling scrap metals. Additionally, this study highlights the importance of precise heat treatments, including homogenization and normalization, by controlling both thermal conditions and the atmosphere to produce high-quality steel from recycled scraps.

Keywords: low-alloyed steel; melting/casting process; induction furnace; thermal treatments; gas phase composition

check for updates

Citation: Ah-lung, G.; Barchid, A.; Boubeker, B.; Samih, Y.; Alami, J.; Senhaji, S.B.; Jacquemin, J. Effects of Melting/Casting and Thermal Treatment Surrounding Gas Phase Composition on the Properties of a Low-Alloyed Steel. *Metals* **2024**, *14*, 1317. https://doi.org/10.3390/met14121317

Academic Editor: Andrea Di Schino

Received: 24 September 2024
Revised: 12 November 2024
Accepted: 18 November 2024
Published: 21 November 2024

Copyright: © 2024 by the authors. Licensee MDPI, Basel, Switzerland. This article is an open access article distributed under the terms and conditions of the Creative Commons Attribution (CC BY) license (https://creativecommons.org/licenses/by/4.0/).

1. Introduction

The realm of metallurgy stands as one of humanity's most ancient domains, universally acknowledged as a branch of applied science. Certainly, metallurgy continues to be a discipline applied extensively on an industrial level, often supported with a research and development (R&D) division. The primary focus of numerous studies is to establish relationships between the chemical composition, heat treatment, resulting microstructures, and corresponding mechanical characteristics of given steels. For example, Tandon et al. studied how variations in heat input through gas tungsten arc welding affect the microstructure, mechanical properties, and corrosion resistance of austenitic stainless steel (ASS) and low-nickel stainless steel (LNSS) [1]. Similarly, El-Bagoury et al. investigated the impact of different alloying elements and heat treatment conditions on the microstructure and properties of Fe–Mn–Al–Cr–C stainless steels [2]. Pacheco et al. focused on how thermal treatments influence the microstructure and performance of duplex stainless steels [3], while Qiao et al. examined the effects of thermomechanical treatment on medium-manganese steels [4]. These studies align with Nasiri et al.'s review on the thermal mechanisms of microstructural refinement in various steels [5], as well as Jorge

et al.'s analysis of the relationship between microstructure and toughness in C–Mn and high-strength low-alloy steel weld metals [6]. A common theme across these works [1–6] is the connection between chemical composition, heat treatments, and the resulting microstructure and properties of specific steel grades. In other words, variations in chemical composition and applied heat treatments during steel manufacturing can directly impact the resulting microstructure, thus affecting their properties [7]. Based on these relationships and the associated understanding, researchers and engineers tend then to select a suitable grade along with its metallurgical route that aligns with specifications frequently applied on an industrial scale. This further demands the development of different strategies that allow a technological transfer from the laboratory (Lab) to industrial manufacturing (Fab) but also from Fab to Lab to Fab.

Furthermore, prior to discussing these strategies, which are designed to scale up from Lab to Fab, allowing the production of the targeted grade at an industrial level, a deeper understanding of the steelmaking process must be brought both at Lab and Fab scales.

On one hand, an industrial steel manufacturing process entails a multi-step sequence respecting a well-designed metallurgical route that involves, generally, primary metallurgy, tapping, secondary metallurgy, continuous casting, rolling (hot and cold), and final thermal treatments processes [8]. In this case, the primary metallurgy involves a careful selection of scrap and raw materials with respect to the desired grades to be melted, resulting in molten steel with a balanced iron and carbon content, which still requires further refinement. An electric arc furnace (EAF) is quite often used to ensure the scraps melting. This first step ends by separating the slags generated during the primary metallurgy (black slag) and the as-melted steel, which is tapped to control the gas concentration in the liquid phase through the addition of deoxidizers (Al, Si, Mn, etc.) and chemical agents (MgO, CaO, etc.), thus inducing the creation of a thick protective slag layer (white slag) onto the deoxidized liquid steel to prevent its further oxidation. Alloying elements can be introduced at this stage to streamline the secondary metallurgy process. The deoxidized steel is then transferred to a ladle furnace (LF) for refining, where additional alloying elements achieve the desired chemical composition [9,10]. Next, the steel is solidified through a continuous casting machine, forming billets, blooms, or slabs under controlled cooling to prevent breakout [11]. The cast steel undergoes a thermal treatment at around 1200 °C before hot-rolling, which yields a uniform austenitic microstructure. Finally, the solidified steel undergoes the rolling (hot and then cold) process followed, generally, by an annealing thermal treatment to provide the final shape and thickness to the product with well-defined relaxed microstructure and homogenized chemical composition.

On the other hand, at a Lab scale, two main strategies are generally employed to provide insights on the relationship between chemical composition, thermal treatment conditions and the resulting microstructures and associated mechanical properties.

The first and prevalent approach used at the Lab scale for exploring and defining these connections typically involves the utilization of an industrial benchmark, followed by conducting various heat treatments and subsequently evaluating the resultant properties on the tested steel grade vs. those determined on the as-received material. These comparative studies generally reported on properties encompassing changes on microstructural and mechanical aspects, and they occasionally extend to specific traits like ballistic performance and corrosion resistance when applying proper heat thermal treatments [12–16]. In this context, Prifti et al. studied the impact of tempering temperature on heat-treated improved rolled homogenous armor (IRHA) steel plates [12]. During this work, a normalization (927 °C and Air cooling) followed by an austenitization at 927 °C and water quenching were performed on the commercial steel. Then, these authors investigated the impact of the tempering temperature on the resulting microstructures and associated mechanical properties of the tested material [12]. The tempering temperature effect on a commercial benchmark was also investigated by Jena et al. on a commercial ultra-high-strength steel (UHSS), where a classical austenitization at 910 °C followed by oil quenching was performed [13]. A similar approach was also followed by El-Bitar et al., who reported on the

impact of the tempering process on a commercialized high-strength steel (HSS) [14]. During this work, these authors reported on the microstructure and the mechanical properties changes of an industrial steel after an austenitization at 910 °C, a water quenching, and different tempering temperatures [14]. Similarly, Paristiawan et al. highlighted the impact of hardening (different quenching methods) and tempering (different temperatures) on an armor laterite steel (ALS) [15]. More recently, Haiko et al. reported on the effect of the applied tempering temperature on a UHSS sheet from SSAB on its resulting mechanical properties, microstructure, dislocation densities, and fracture surfaces [16]. This first approach was also deeply applied on various dual phase (DP) steels, as these materials have gained strong interest over the last decades, especially in the automotive industry due their exceptional mechanical attributes, which encompass remarkable tensile strength, outstanding resistance to both ductile and brittle fractures, and notable deformability owing to their low yield strength [17–20]. The majority of these studies focused on enhancing the performance of DP steels by following a similar strategy, which involves carrying out proper heat treatments on commercially available steel sheets typically produced through hot and/or cold rolling processes [17–20]. For example, Alibeyki et al. investigated the effect of the intercritical annealing on the final microstructure and the associated mechanical properties of low-carbon steel sheets available on the market [17]. Moreover, various methods for producing DP steels are also outlined in the existing literature [18]. Intercritical quenching (IQ), intercritical annealing (IA), and step quenching (SQ) are three commonly applied treatments. In this regard, Soleimani et al. studied the mechanical and corrosion characteristics of low-carbon steel sheets utilizing distinct processing pathways, IA, and SQ [19]. Balbi et al. conducted a deeper investigation on the IA of a ferrite-martensite DP steel [20]. The impact of the holding time on both the final microstructure of DP steels and associated tensile properties was also clearly highlighted by following a similar approach [20]. Weathering steel (WS) is low-alloyed steel widely recognized and utilized for its notable ability to resist atmospheric corrosion [21]. This type of steel is widely recognized and is subjected to stringent standardization, especially in terms of chemical composition. However, recent studies evaluated the impact of other elements on their performances regarding the mechanical and corrosion behavior aspects [22–24]. Despite the focus on chemical composition in these investigations, the main approach remains consistent, involving the use of commercial plates [22,23]. For example, the effect of silicon on the corrosion resistance of a reference steel was investigated by doping the benchmark with different Si contents. The corrosion resistance of each steel was then compared to the commercial benchmark used as the reference sample [22]. More recently, Chen et al. reported novel insights with respect to the impact of silicon on the corrosion resistance by the formation of a three-dimensional SiO_2 network by using plates supplied by the China HBIS group [23]. A similar approach was also followed by Cano et al. to understand the effect of the addition of Cr, Cu, and Ni on the corrosion resistance behavior of a benchmark weathering steel in a marine atmosphere [24].

The second approach applied at the Lab scale consists of making the steel using different technologies of steelmaking. Before delving into the details of these endeavors, it is crucial to emphasize that a diverse spectrum of scales is encompassed, ranging from laboratory settings and pilot projects to full industrial implementation. As described previously, the most common system recently used in industry is the combination of EAF and LF. However, to rapidly produce a grade of steel, an alternative technology based on the induction process is usually used [25]. Among the well-established technologies, steel grades can be produced from scrap metals using an EAF and LF steelmaking process [26,27]. However, when iron ores and metallurgical coke are used as raw materials a blast furnace (BF) associated with a basic oxygen furnace (BOF) is generally preferred. Schrama et al. reviewed the elimination of sulfur during the ironmaking and oxygen steelmaking processes taking place on an industrial level [26]. An induction furnace was used to replicate a part of the process, including the tundish located between the EAF and the LF to validate the selected setup and the industrial level [27]. Kukartsev et al. used an induction furnace to investigate

the smelt ability of some scraps for the production of cast iron and steel materials [28]. They tested several parameters such as the frequency and the melting mode and presented the advantages and disadvantages of using melting induction technology [28]. Gertsyk and Mineev from Moscow Polytechnic University developed an induction unit, with a capacity of 1100 kg, for the production of structural cryogenic 12Kh18N10T stainless steel from industrial waste [29]. An induction furnace associated within a periclase lining was also used by Serov et al. to investigate the effect of deoxidation on the composition of non-metallic inclusion in pipe steels, for example [30]. An LSZ-35 induction furnace was used by Osei et al. to mimic the industrial scale formation during reheating and the impact of the copper content in a low-carbon steel [31]. These authors reproduced the natural gas combustion atmosphere present in an industrial furnace [31]. In summary, the technologies used for steelmaking at the different scales are used without an understanding of the optimal conditions to be set to reach desired properties. Therefore, our study stems from the examination of various parameters related to the melting and casting process at the lab scale. In the present study, an appropriate strategy combining academic and industrial scientists was initiated and implemented for ensuring an efficient transition from Lab to Fab scale by using facilities available at the Accelerated Research Centre for Metallurgy laboratory combining Maghreb Steel and the Mohamed VI Polytechnic University facilities (see Table S1 of the Electronic Supporting Information (ESI)). This strategy is based on the utilization of an induction technology, selected for its ability to be employed both as an EAF and/or a LF under rigorous melting and casting conditions. Moreover, since the EAF is usually mastered at the industrial scale, using the vacuum induction melting (VIM) furnace as a LF is the most suitable approach to ensure a fast Lab to Fab transition. However, this strategy requests a strong understanding of the different processes and parameters to be applied on each device and technology used at both Lab and Fab scales.

The aim of this study is to explore the scraps recycling capability in steel production. To achieve this, a benchmark low-alloyed steel, commercially known as PROTAC®, was selected to investigate the impact of multiple melting/casting cycles on its chemical composition under different atmospheres (vacuum, argon, and air) using a vacuum induction furnace. This approach evaluates how the recycling process affects the material's properties. Following the melting/casting cycles, various standard heat treatments—including homogenization, normalization, and different cooling or quenching methods—were applied to each sample using a conventional furnace (in ambient air). Additionally, similar thermal treatments were conducted in a vacuum induction furnace with a controlled atmosphere to assess the influence of the surrounding atmosphere on the material's properties. By comparing these results with literature data for this commercial steel grade [32,33], the study provides insights into how different steelmaking conditions affect the chemical composition, microstructure, and hardness of low-alloyed steels. The comparison considers the as-received plate, existing literature [32,33], and the conditions applied herein, underscoring the importance of optimizing steelmaking processes to maintain desirable steel properties. Furthermore, various scrap metals corresponding to other low-alloyed steel grades were utilized to support these findings, with the materials used and their recyclability results reported in Case Studies Section of the ESI.

2. Materials and Methods

2.1. Materials Used and Conditions Applied

A commercial plate of PROTAC 500® with the dimensions of (1000 × 1000 × 8) mm of a low-alloyed steel produced by SIJ Acroni© company located in Jesenice, Slovenia was investigated in the present work. This as-received material was partially cut off into small pieces with dimensions of (100 × 40 × 8) mm. Then, approximately 400 g of this steel grade was placed inside a zirconia crucible prior to being melted and casted, through multiple cycles (up to 5) under different atmospheres (air or Ar under low or atmospheric pressures), using a TVM15-Vac2 induction furnace from TOPCAST© (Monte San Savino, Italy). The connected pyrometer is a Pyrospot DSR 55NV from Dias Infrared Systems,

allowing the measurement of the scrap metals temperature placed inside the zirconia crucible from 800 °C to 2500 °C with a resolution of 0.5% of measured value (in °C) plus 1 K (min = 5; max = 13.5). The manometer was an ISE20C, provided by SMC, allowing a gage measurement from −0.1 to 1 MPa with a resolution of maximum 2%. Prior to melting and casting the steel/scraps, and even after the vacuum cycles, a step of preheating, at 900 °C, was systematically performed. At this stage, the quantity of oxygen was always lower than 10 ppm when working under vacuum or under argon (i.e., except for the melting/casting made under air). A large drop on O_2 concentration was subsequently noted, reaching a reading range of [10^{-14}–10^{-17}] ppm, which was, in fact, far below the detection limit of our equipment, thus indicating a quantity of oxygen lower than 1 ppm. Consequently, the oxidative reactions that may occur through the melting/casting process realized under vacuum or argon conditions would be performed with an amount of oxygen lower than 10 ppm. The melting process was visually observed upon reaching a temperature close to 1500 °C, while the time required depended mainly on the magnetic properties of the scrap metals being melted. The molten liquid was then cast gravitationally into a copper mold (approximately 150 × 150 × 150 mm, with a copper thickness of 10 mm), resulting in a specimen of approximately 100 × 100 × 5 mm, depending on the quantity of scrap metal used. The mold was made of copper to achieve high thermal conductivity, allowing for rapid dissipation of thermal energy and preventing brazing effects. Subsequently, heat treatments for homogenization (1100 °C for 30 min) and normalization (900 °C for 30 min) were performed on each as-cast specimen in the TVM15-Vac2 or in a standard muffle furnace from JP Selecta© (Model Select-Horn-TFT, Barcelona, Spain), as shown in Figure 1. Different cooling steps were then applied directly in the respective furnace (furnace quenching—FQ; slow cooling rate—0.02 °C.s^{-1}), under air (air quenching—AQ; intermediate cooling rate—[30–50] °C.s^{-1}) and a homemade quenching bath filled with water (water quenching—WQ; fast cooling rate—100 °C.s^{-1}; the volume was considered infinitely higher than the sample volume, preventing any temperature increase in the water bath used).

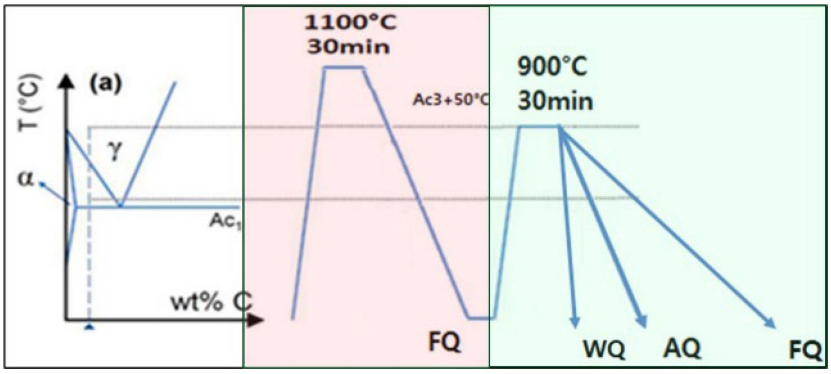

Figure 1. Schematic representation of the different heat treatment cycles investigated during this study, corresponding to the homogenization (1100 °C) and normalization (900 °C) heat treatments, along with the subsequent quenching method applied (FQ, WQ, or AQ).

In addition, to further exemplify the possibility of recycling scrap metals using an induction furnace under a controlled atmosphere (vacuum) to produce various low-alloyed steel grades without any refinement process, a melting/casting cycle was applied to produce three other steel grades at the kg scale. The results related to the chemical composition of the scraps used during each melting/casting process, along with the chemical composition and microstructure achieved after the homogenization and normalization heat treatments, are reported in the ESI.

2.2. Characterization Technique

2.2.1. Chemical Reagents/Etching Agents

In this study, few chemical reagents were used, being employed mainly for preparing the etching solution, like the ethanol (EtOH, 96%, CAS 64-17-5) and nitric acid (HNO_3, 68–70%, CAS 7697-37-2), both purchased from Sigma Aldrich, which were used to prepare the Nital 5% solution (EtOH-HNO_3; *v*:*v* % = 95:5).

2.2.2. Chemical Composition

The chemical analyses of the as-received and as-prepared samples were carried out using an ultra-compact and versatile optical emission spectrometer (OES) S1 Minilab 150 from GNR France© (Marnay, France). This equipment is used primarily for the analysis of metal content based on the OES principle. Briefly, during each OES measurement, a small steel specimen was prepared by grinding to ensure a clean, flat surface for analysis. It was then placed in the spectrometer, where a high-voltage spark under an Ar atmosphere vaporized a portion, creating a plasma. This plasma emitted light with characteristic wavelengths of the elements present. An optical system directed this light through a diffraction grating, separating it into spectral components, which were recorded by a CCD detector. The recorded spectrum was analyzed to determine element concentrations, with calibration curves from reference materials ensuring the accuracy of the measurements. For this reason, prior to running the experiment, the instrument was calibrated by using standard samples as preconized by the supplier to ensure the reproducibility of the data within a maximum error of 0.01% for regular elements and 0.1% for non-conventional elements or ones that can be detected as impurities or tracks. The accuracy of each reported composition is ensured by assessing the sensitivity of their determination in a certified material (see Figure S1 of the ESI).

The content of each element in a given steel sample was measured several times for each investigated condition and trial. The reproducibility and the consistency of the claimed results are supported by the average measurements in different zones, as shown as an example in Table S2 of the ESI.

2.2.3. Microstructures

To unveil the microstructure, specimens were prepared by mounting and polishing (Presslam 1.1 and Smartlam 1.1 provided by Lam Plan®, Gaillard, France) until a reflective surface was achieved. Subsequently, the samples underwent etching with the prepared Nital solution. Initial microstructural observations were conducted using an optical microscope (OM) (Eclipse LV 100 ND by NIKON©, Champigny sur Marne, France). Based on the optical clichés, phase repartition and grain size were measured using ImageJ software (version 1.54d). Further and detailed analyses were carried out using the ZEISS© EVO 10 scanning electron microscope (SEM, Cambridge, UK) equipped with the integrated SMART EDS detector, using an acceleration voltage of 15 kV, a probe current of 1 nA, and a working distance of 10 mm.

2.2.4. Hardness

Hardness measurements were carried out using an AFFRI© Rockwell 206 EX/MX hardness tester (Varese, Italy). The measurements utilized a Rockwell indenter and were later transformed into Brinell hardness (HB) values. The hardness tester was initially calibrated using a standard sample HRC 58.9 (see Figure S2 of the ESI). The as-measured hardness data are provided with a maximum error of 1.5%, and each single datum was repeated at least three times with respect to each investigated sample. Similarly to the chemical composition measurement, the given values of hardness cited in the present work were an average of different measurement points (see Table S2 of the ESI).

2.2.5. Dilatometry

The dilatometry measurements were conducted with a fully automated quenching dilatometer LINSEIS© (L78 RITA Q, Selb, Germany) to study the phase transformations. This instrument was equipped with a linear variable differential transformer (LVDT) sensor that measures the dimensional changes of the samples with a resolution of $\Delta L/°C = 0.01\ \mu m/0.05\ °C$ when measuring length change and performed under extremely controlled heating and cooling conditions. The temperature of the specimen was measured and controlled with a K-type thermocouple spot welded at the center of the specimen surface. The dilatometer machine was equipped with an induction furnace and gas control unit (type L78 QD GASBOX), which allows precise control of heating and cooling steps. The steel samples used for the different thermal cycles executed in dilatometry were cut and machined from homogenized and normalized ingots to reach standard specimen sizes of 3 mm diameter and 10 mm length. To examine the critical transformation temperatures during the heating and cooling of each steel sample, several thermal treatments were applied under helium gas. All tested samples were first heated from room temperature (approximately 30 °C) to an austenitization temperature of 950 °C with a constant heating rate equal to 10 $°C.s^{-1}$. After a holding time of 50 s at this temperature, a constant cooling rate was applied down to room temperature. Therein, 4 cooling rates, close to 10 $°C.s^{-1}$, 1 $°C.s^{-1}$, 0.1 $°C.s^{-1}$, and 0.02 $°C.s^{-1}$, were applied to the sample by using gas quenching to study the effect of cooling rate on dilatation curves. The A_{c1} and A_{c3} temperatures were then identified from the change in length versus temperature curves using the tangential extrapolation method applied to the linear segments of the dilatation versus temperature plots ($\Delta L/Lo$ vs. T) when increasing the temperature up to 950 °C. Dilatometry measurements performed in cooling mode were then used to identify the phase change temperature and thus the microstructure obtained as a function of investigated cooling rates.

3. Results and Discussion

3.1. Characterization of a Benchmark—PROTAC 500® Low-Alloyed Steel

Herein, the investigated steel grade was the PROTAC 500® produced by SIJ Acroni© in Slovenia. It is important to note that this sample was received as a non-conform sample. The as-received plate was cut-off into smaller plates, and the chemical composition of several plates was investigated both at the surface and bulk, as reported in Table 1 and in Table S2 of the ESI. The carbon and the manganese contents in each tested zone were always lower than the expected values claimed by the supplier as well as those reported by Cabrilo et al. [32,33]. One should note that the results of the chemical composition of the surface were different when compared with the values of the bulk, showing that the PROTAC 500® sample was not homogeneous and in fact was not conform. Based on this observation, the main objective of this study was then to investigate the best conditions to make it conform.

To further investigate such composition differences, the microstructure of the as-received sample was analyzed at both the surface and the cross-section by using scanning electron microscopy (SEM). As shown in Figure 2a,b, both analyses revealed a typical bainitic-martensitic microstructure in alignment with the hardness measurements (495 HB) reported in Table 1. A fully martensitic microstructure should have exhibited a higher hardness (>500 HB), confirming the obtention of a proportion of bainite. However, one can also detect the presence of precipitates particularly located in the cross-section. According to the EDS analysis (Figure 2c where C content was estimated), these precipitates were enriched with carbon and manganese, explaining the drop observed for these elements in the chemical composition of the as-received sample (Table 1).

Table 1. Chemical composition (in wt.%) and hardness of the standard (low-alloyed steel), as-received steel, values issued from the literature, and max values of commercials grades.

Material	Composition (wt.%)								HB	Ref.
	C	Mn	Si	Cr	Ni	Mo	Cu	Fe		
Low-alloyed steel—certificate values	0.403	0.416	0.295	0.187	1.502	0.184	0.360	Balance	NA	Supplier *
Standard low-alloyed steel—measurements	0.419	0.417	0.299	0.192	1.471	0.179	0.352		NA	This work
PROTAC 500®—surface	0.149	0.534	0.971	0.464	1.033	0.370	0.154		495	This work
PROTAC 500®—bulk	0.302	0.525	0.940	0.459	1.007	0.357	0.155		420	This work
PROTAC 500® (Literature)	0.270	0.710	1.070	0.640	1.090	0.300	0.154		464	[32,33]
PROTAC 500® (supplier, max in wt.%)	0.300	0.800	1.300	−0.800	1.500	0.500	-		480–530	Commercial datasheet

* Values were taken from the certificate of analysis of a certified reference material, SS-CRM No. 114, with measurements performed by the Bureau of Analysed Samples (BAS) Ltd. (Middlesbrough, UK). This reference material was used to verify the calibration of our equipment for a given range of steel chemical compositions, reflecting the investigated grade—in this case, a low-alloyed steel (see Figure S1 of the ESI).

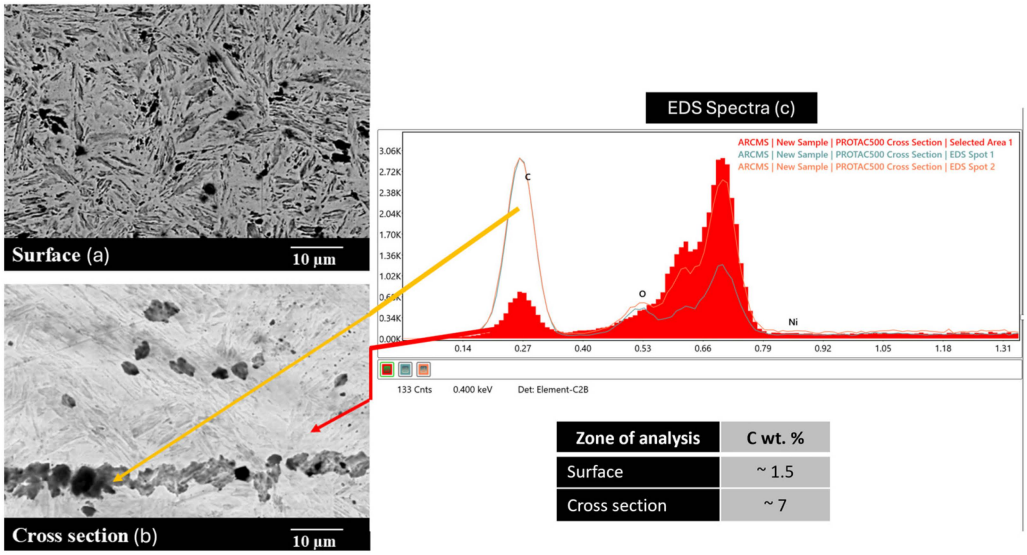

Figure 2. SEM images of both (**a**) the surface and (**b**) the cross-section of the as-received sample and (**c**) the EDS spectra of investigated zones.

Usually two types of Mn-carbides can be identified in a low-alloyed steel. Cementite-like carbides (Mn_3C or $(Fe,Mn)_3C$) are typically formed around 450 °C, accompanied by a slow cooling rate [34–36]. The second type of carbides are Mn_7C_3 and $Mn_{23}C_6$ that usually precipitate in heat-affected zones (HAZ), typically a welded area [34,35]. However, based on the SEM/EDS analysis (Figure 2c), a higher amount of carbon of about 7 wt.% was measured for the observed precipitates in comparison with the top surface (1.5 wt.%). The carbon quantification by EDS was obviously not accurate (overestimation of carbon wt.% due to the surface contamination) but still allowed us to compare qualitatively the difference between the surface and the bulk.

Consequently, the hypothesis of carbide formation was rejected, and it was concluded that segregation of carbon atoms occurred around manganese located in the rolling lines. Furthermore, it was demonstrated that the segregation of carbon occurred though a continuous casting process [37–39]. This defect, called centerline macro-segregation, generally occurs in the bulk center, as highlighted in the SEM image of the bulk cross-section reported in Figure 2b [40]. The results described above show that the as-received material was a semi-final product, and it was assumed that this segregation phenomena could be

responsible for such chemical composition differences between the sample surface and bulk, and more importantly, with the composition expected for such a commercial grade. Based on the data reported in Table 1, it is also noticeable that the nickel content was higher than the maximum value reported in the supplier datasheet, but all Ni-based measured values were consistent with those reported by Cabrilo et al. [32,33].

3.2. Impact of the Homogenization and Normalization of the As-Received Sample on the Re-Solubilization of the Carbides Using an Induction Furnace (VIM)

The first step of the study was to investigate the feasibility of dissolving the identified precipitates through a homogenization process, utilizing an induction furnace under a vacuum or inert atmosphere to prevent decarburization. To achieve this, one of the cut plates was placed in the VIM furnace and heat-treated at 1100 °C under an inert argon atmosphere for 30 min, ensuring that the precipitates within the bulk of the material were effectively reached. The temperature of 1100 °C was chosen based on the commercial steel's carbon content (0.3 wt.%) and to align with typical industrial thermal treatment temperatures prior to hot rolling. Following this treatment, the plate was cooled inside the furnace, and the resulting chemical composition is presented in Table 2. One can notice the impact of such a thermal treatment on the carbon content, where the carbon increased from 0.149 wt.% before homogenization to approximately 0.256 wt.% after this treatment. Such a result demonstrates the re-solubilization of the identified precipitates in the previous part. Moreover, one can notice that only the carbon content re-increased, e.g., the Mn content remained constant as the precipitates corresponded to the segregation of carbon around Mn in the centerline of the material.

Table 2. Chemical composition (in weight %) and hardness before and after homogenization in the VIM furnace.

Material	Composition (wt.%)								HB
	C	Mn	Si	Cr	Ni	Mo	Cu	Fe	
Before homogenization	0.149	0.534	0.971	0.464	1.033	0.370	0.154	Bal.	464
After homogenization	0.256	0.540	1.170	0.467	1.097	0.377	0.159	Bal.	215

The microstructure analyzed through optical microscopy (OM) and scanning electron microscopy (SEM) after homogenization is shown in Figure 3. These images clearly indicate that the homogenization treatment was successful, as all the precipitates initially present in the bulk were dissolved. Additionally, the surface exhibited ferrite and bainite-like microstructures after homogenization (Figure 3a,b), which aligns with the measured hardness of 215 HB reported in Table 2. This outcome was anticipated since the homogenization treatment was followed by a slow cooling rate inside the furnace. In contrast, the bulk of the material displayed a bainitic microstructure (Figure 3c,d). Such a difference can be due to carbon concentration differences between the surface and in the bulk, as it may shift the bainite transformation range and influence the transformation rate.

After conducting the homogenization, a normalization heat treatment is always performed. In industry, this normalization treatment is conventionally set at 50 °C above the Ac_3 critical temperature, especially when this temperature is calculated according to the following formula (Equation (1)) [41]:

$$A_{c3} = 925 - 219\sqrt{C} - 7\,Mn + 39\,Si - 16\,Ni + 13\,Mo + 97\,V \quad (1)$$

Based on the chemical composition of our samples, a target temperature of 900 °C was established. Dilatometry measurements were then conducted to validate this calculated temperature to be applied during the normalization heat treatment. The dilatometry results, presented in Figure 4, show the heating profile obtained with the as-received sample after homogenization (i.e., avoiding the segregation issue highlighted in Section 3.1). From

this heating profile, Ac_1 and Ac_3 were determined to be close to 755 °C and 865 °C, respectively. Therefore, a temperature of 900 °C should be sufficient for normalizing the normalized sample.

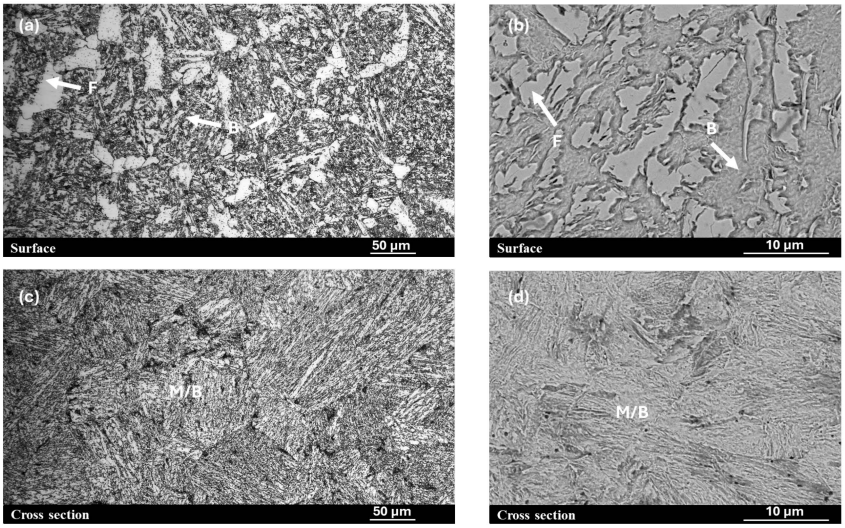

Figure 3. OM and SEM images of both the surface (**a**,**b**) and cross-section (**c**,**d**) of the as-received sample after its homogenization at 1100 °C in the VIM furnace under inert atmosphere (argon) for 30 min.

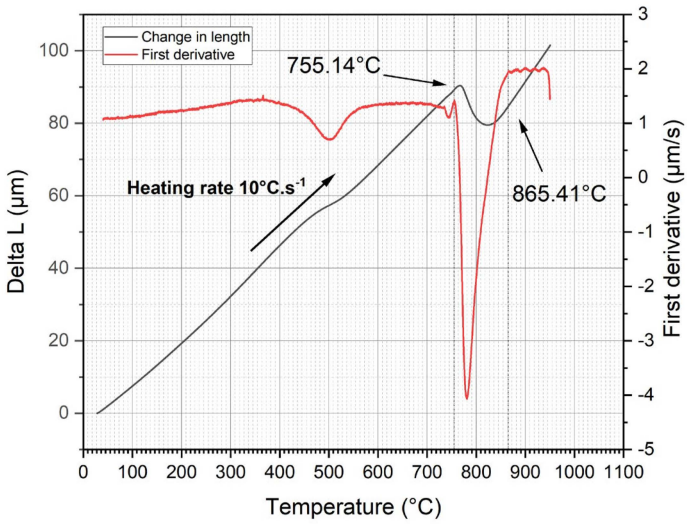

Figure 4. Dilatometry heating curve of the samples after the austenitization temperature up to 950 °C with a constant heating rate equal to 10 °C.s^{-1}.

Consequently, homogenized samples were then normalized at 900 °C for 30 min inside the VIM furnace under argon prior to slowly cooling the sample again in the furnace. The obtained microstructure, shown in the OM in Figure 5, highlights the presence of the bainite-like microstructure at both the surface and the bulk of the sample.

After this normalization treatment, the hardness of the tested steel increased from 215 HB to 230 HB due to the refinement of the grains. Moreover, one can notice that the segregation of carbon atoms did not occur after the applied normalization, thus confirming that the initial segregation problem, observed with the as-received sample (Figure 2), could be associated within the manufacturing process, notably during the continuous casting step.

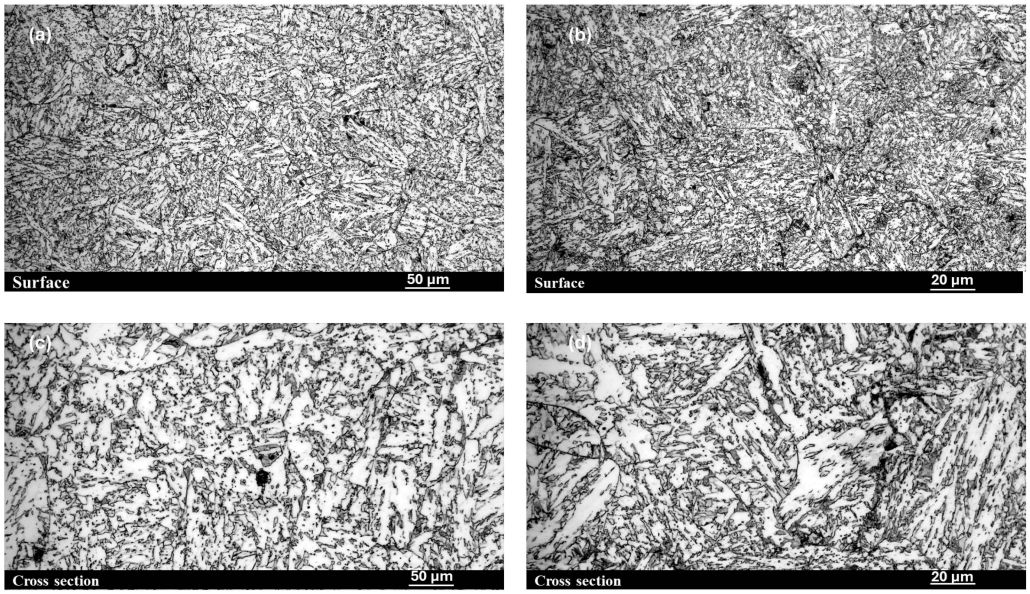

Figure 5. OM images at 2 magnifications of both the surface (**a**,**b**) and cross-section (**c**,**d**) of the as-received homogenized sample after its normalization at 900 °C in the VIM furnace under inert atmosphere (argon) for 30 min.

3.3. Impact of the Atmosphere on the Chemical Composition Through Melting/Casting Cycles Using an Induction Furnace (VIM)

The second phase of this study involves employing the VIM furnace to recycle the as-received and non-conforming steel plate to cast new plates. Additionally, this phase sought to examine how various atmospheres affect the chemical stability of the casted plates across multiple melting and casting cycles. During this study, the selected atmospheres were respectively named vacuum (e.g., 200 mbar of argon), argon (1 bar of argon), and air (1 bar of air), which all followed a proper vacuum cycle to prepare the steel prior to its melting, as displayed in Figure 6.

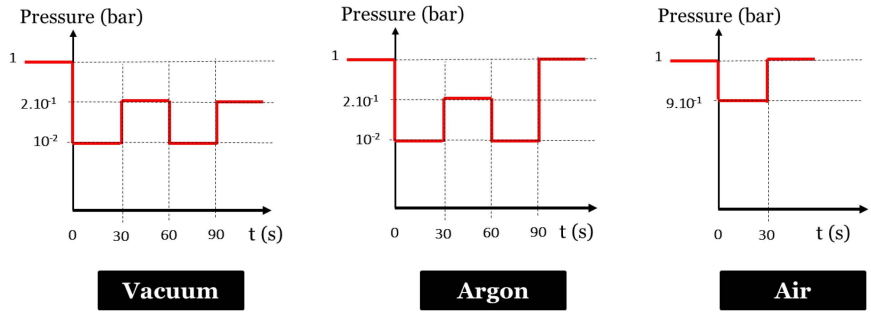

Figure 6. Applied vacuum cycles to control the atmosphere inside the VIM chamber prior to melting the steel sample.

As shown in the latter figure, the atmosphere herein called "vacuum" corresponds to a well-controlled low-pressure atmosphere containing solely argon. This pressure value (e.g., 200 mbar of argon) was selected with respect to the condition of utilization of the VIM furnace. This pressure level corresponded to the lowest pressure value for conducting a proper melting/casting process able to prevent sparking liquid steel and consequently projection out of the crucible. With respect to the targeted atmosphere, each cycle reported in Figure 6 was performed prior to activating the induction generator. For such a type of steel, its melting occurs after 20 min under induction. After each melting, the material was then casted gravitationally in a (100 × 100 × 100) mm copper mold placed inside the VIM furnace prior to being analyzed and then subsequently melted and casted again to evaluate

the effects of both the selected atmosphere and the number of melting/casting cycles on the recyclability of the tested material by considering the law of conservation of mass as a probe.

By following such a strategy, the mass evolution of the tested materials along with the five applied melting/casting cycles for each targeted atmosphere was as depicted in Table 3.

Table 3. Mass evolution through melting/casting cycles under the three tested atmospheres.

Condition	**Vacuum**					**Argon**					**Air**		
Casting n°	**1**	**2**	**3**	**4**	**5**	**1**	**2**	**3**	**4**	**5**	**1**	**2**	**3**
$m_{initial}$ (g)	559.0	538.4	537.0	523.5	512.7	427.8	411.9	403.1	388.9	361.7	454.9	No melting after 3 h in the VIM	
m_{final} (g)	557.5	537.9	534.4	523.4	502.5	425.8	409.1	401.5	371.1	360.3	439.8		
Loss (%)	0.27	0.09	0.48	0.02	2.0	0.47	0.68	0.40	4.6	0.39	3.3		

Under a controlled atmosphere, either vacuum or argon, the mass retention was excellent (generally better than 1%) between each melting/casting cycle, demonstrating the recyclability of the tested material. This effectiveness is attributed to the well-controlled atmosphere, which prevents the oxidation of the chemical elements present in the steel. The highest mass retention values—2.0% observed under vacuum (casting n° 5) and 3.1% under argon (casting n° 4)—can be easily explained by the presence of some residues inside the copper mold after demolding. However, by melting/casting under air atmosphere, an initial 3.3% mass loss was observed immediately after the initial casting. Very surprisingly, even after a 3 h induction period in the chamber at the maximum induction power, the melting did not occur for the subsequent melting/casting cycle under air. In other words, it was impossible to remelt the material after its first melting/casting cycle when using air as the VIM atmosphere. Consequently, the initial 3.3% mass loss can be easily associated with a loss of elements contributing to the magnetic property of the tested steel, where such a property is necessary for responding to the induction power applied in the used zirconia crucible, limiting the possibility to further recycle the material under applied conditions. However, in such cases, another crucible material, such as graphite, should be used to ensure the melting of the scraps. This aspect was not investigated here, as the main objective was to study the impact of the atmosphere on the consecutive melting and casting of scrap metals and their effects on the resulting chemical composition.

The chemical composition of each as-casted steel material was systematically measured after each melting/casting cycle for all set conditions investigated therein, with data summarized in Table 4. Whatever the set atmosphere, by comparing the carbon content onto the surface of the as-received sample with the value determined after the first melting/casting cycle, it can be noticed that the re-homogenization of the matrix was a success, thus solving the initial observed issue related to the carbon segregation problem observed in the bulk, as shown in Figure 2.

Furthermore, in the case of cycles performed under vacuum, a stabilization of the carbon content was observed after the third melting/casting cycle. Based on this observation, the weight change observed on each element was then calculated between the third and the fourth melting/casting cycles performed under an inert atmosphere, i.e., vacuum or argon, by using the Equation (2):

$$Weight\ Change\ (\%) = 100 \times \left(\frac{w\%_{element}(casting\ n^{\circ}4) - w\%_{element}(casting\ n^{\circ}3)}{w\%_{element}(casting\ n^{\circ}3)} \right) \quad (2)$$

However, in the case of the cycle performed under air, data were solely compared with those determined using the as-received sample as it was impossible to melt the material again after the first melting/casting cycle. All associated results are depicted in Table 5, along with weight change on each element to highlight the impact of the melting/casting atmosphere onto the chemical composition of the tested material.

Table 4. Chemical composition (in weight %) before and after homogenization in the VIM furnace.

Condition	Cast n°	Composition (wt.%)										
		C	Mn	Si	Cr	Ni	Mo	Cu	Nb	P	Bal. Fe	Other
As-received		0.143	0.535	0.982	0.465	1.035	0.371	0.154	0.019	0.005	96.088	0.203
Vacuum	1	0.208	0.518	1.052	0.467	1.114	0.403	0.155	0.022	0.007	95.692	1.362
	2	0.262	0.558	0.818	0.455	1.137	0.371	0.137	0.017	0.012	96.050	0.183
	3	0.252	0.486	1.025	0.458	1.093	0.377	0.152	0.016	0.007	95.853	0.281
	4	0.257	0.441	1.005	0.463	1.099	0.391	0.148	0.020	0.007	95.787	0.382
	5	0.249	0.436	1.127	0.471	1.148	0.397	0.150	0.019	0.008	95.837	0.158
As-received		0.143	0.535	0.982	0.465	1.035	0.371	0.154	0.019	0.005	96.088	0.203
Argon	1	0.181	0.505	0.961	0.470	1.070	0.373	0.161	0.019	0.007	96.111	0.142
	2	0.254	0.489	1.041	0.471	1.041	0.372	0.158	0.020	0.007	95.948	0.199
	3	0.234	0.476	1.051	0.463	1.051	0.362	0.156	0.017	0.006	96.115	0.205
	4	0.219	0.442	0.886	0.459	1.039	0.355	0.151	0.015	0.006	96.283	0.145
	5	0.230	0.426	0.908	0.468	1.062	0.375	0.150	0.018	0.007	96.215	0.141
As-received		0.143	0.535	0.982	0.465	1.035	0.371	0.154	0.019	0.005	96.088	0.203
Air	1	0.227	0.159	0.247	0.362	1.063	0.374	0.160	0.007	0.006	97.259	0.598
	2	No melting after 3 h in the VIM										
	3											

Table 5. Weight change on each element between the third and fourth melting/casting cycles performed under vacuum or argon and between data collected on the as-received plate and the first casting performed under air.

Condition	Weight Change (%)							
	C	Mn	Si	Cr	Ni	Mo	Cu	Bal. Fe
Vacuum	+1.98	−9.26	−1.95	+1.09	+0.55	+3.71	−2.63	−0.07
Argon	−6.41	−7.14	−15.7	−0.86	−1.14	−1.93	−3.21	+0.17
Air	+58.7	−70.3	−74.9	−22.2	−2.71	+0.81	+3.90	+1.22

Under air atmosphere, the weight change was clearly negative for all elements except for carbon, due to the initial carbon segregation problem, as well as copper and molybdenum, due to their weaker affinity with oxygen as expected when looking at the Ellingham diagram [42]. However, under argon atmosphere, the manganese and silicon contents mainly seemed to be strongly affected by the melting/casting cycle, as weight losses up to 7% and 16% were observed for these two metals, respectively. This phenomenon, usually observed without a controlled atmosphere, is called loss by flame [43]. A similar observation was made when melting/casting under vacuum condition in the case of the manganese content, with a weight loss close to 9.3%, while the content of other tested elements seemed to be constant within an accuracy close to 2%. Trace elements, like niobium and phosphorous are really specifics, since their initial content is very low (i.e., lower than 0.02 wt.%), and a small weigh change will, in fact, induce a strong change on weight change when using Equation (2), explaining why they are not reported in Table 5 nor discussed therein.

An observation of the freshly casted plate microstructure was then conducted by using optical and electronical microscopies, and the resulting clichés are depicted in Figure 7.

As a reminder, the steel was heated and melted at 1500 °C before being poured into a copper mold for cooling and solidifying. At this stage, no defined microstructure should be expected for the material produced, particularly when following a gravity die casting process. This was evident in most SEM images, where no clear microstructures, such as ferrite and pearlite (which are expected for this type of steel at equilibrium), could be identified. However, in the case of the plate produced after the first casting under vacuum, a distinct martensitic microstructure was observed [44,45]. This metastable microstructure typically arises from rapid cooling [46,47]. In certain instances, especially when the carbon content exceeds 0.25 wt.%, martensite can form at the steel's surface due to thermal stresses, such as those induced by fast pouring, which creates a temperature difference between the molten steel and the copper mold. These findings underscore the significance of utilizing

a controlled atmosphere, like vacuum, during the melting and casting processes, as it enhances the potential for achieving desirable microstructures and maintains the integrity of the recycled material. Furthermore, they indicate that identifying the microstructure and chemical composition of a freshly cast plate is challenging since the elements have not had sufficient time to diffuse throughout the matrix. As a result, obtaining a well-defined and homogenized chemical composition and microstructure is not feasible at this stage. Therefore, the first thermal treatment necessary for freshly cast material is a homogenization heat treatment, which is crucial for optimizing the properties of recycled steel.

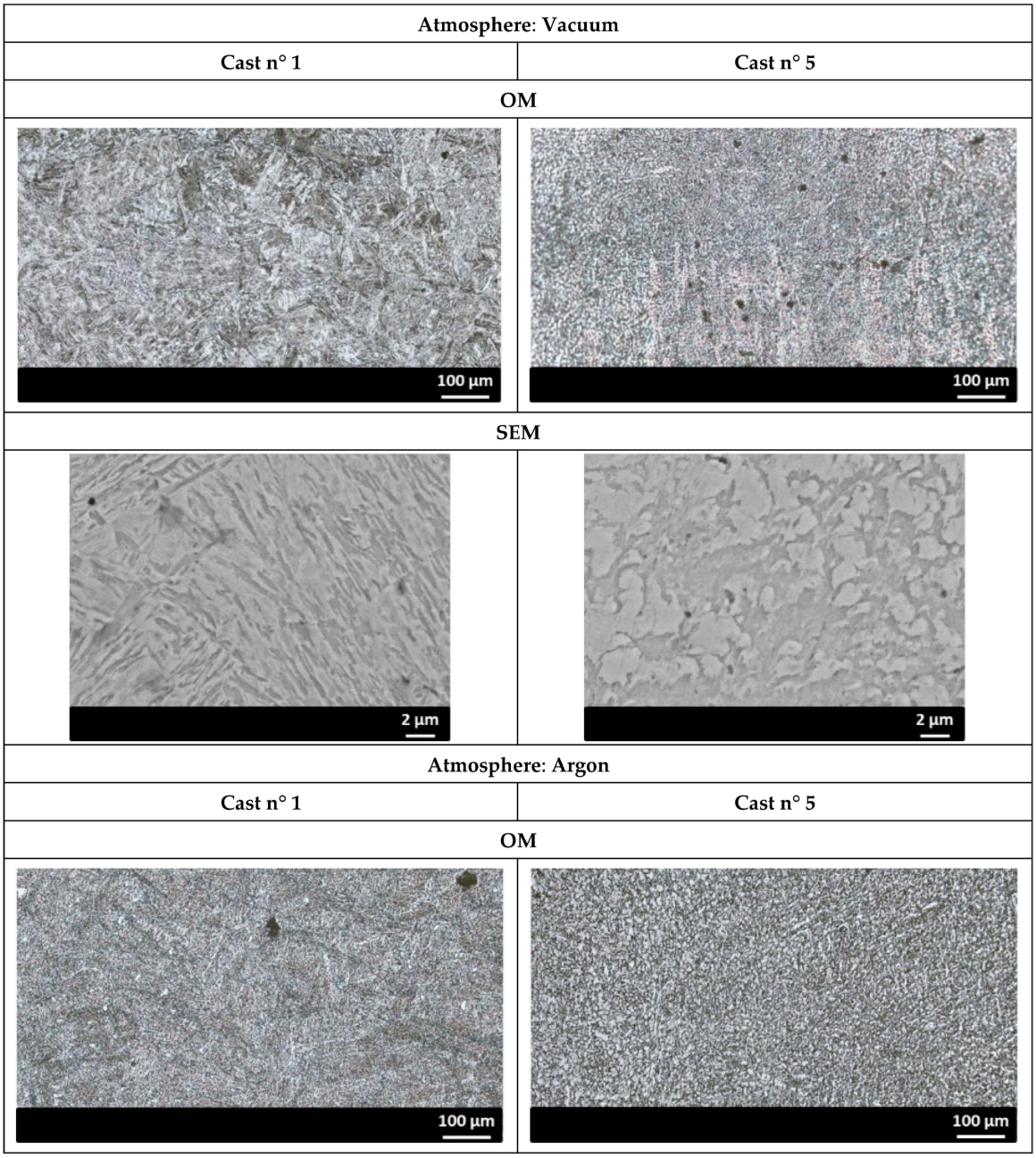

Figure 7. *Cont.*

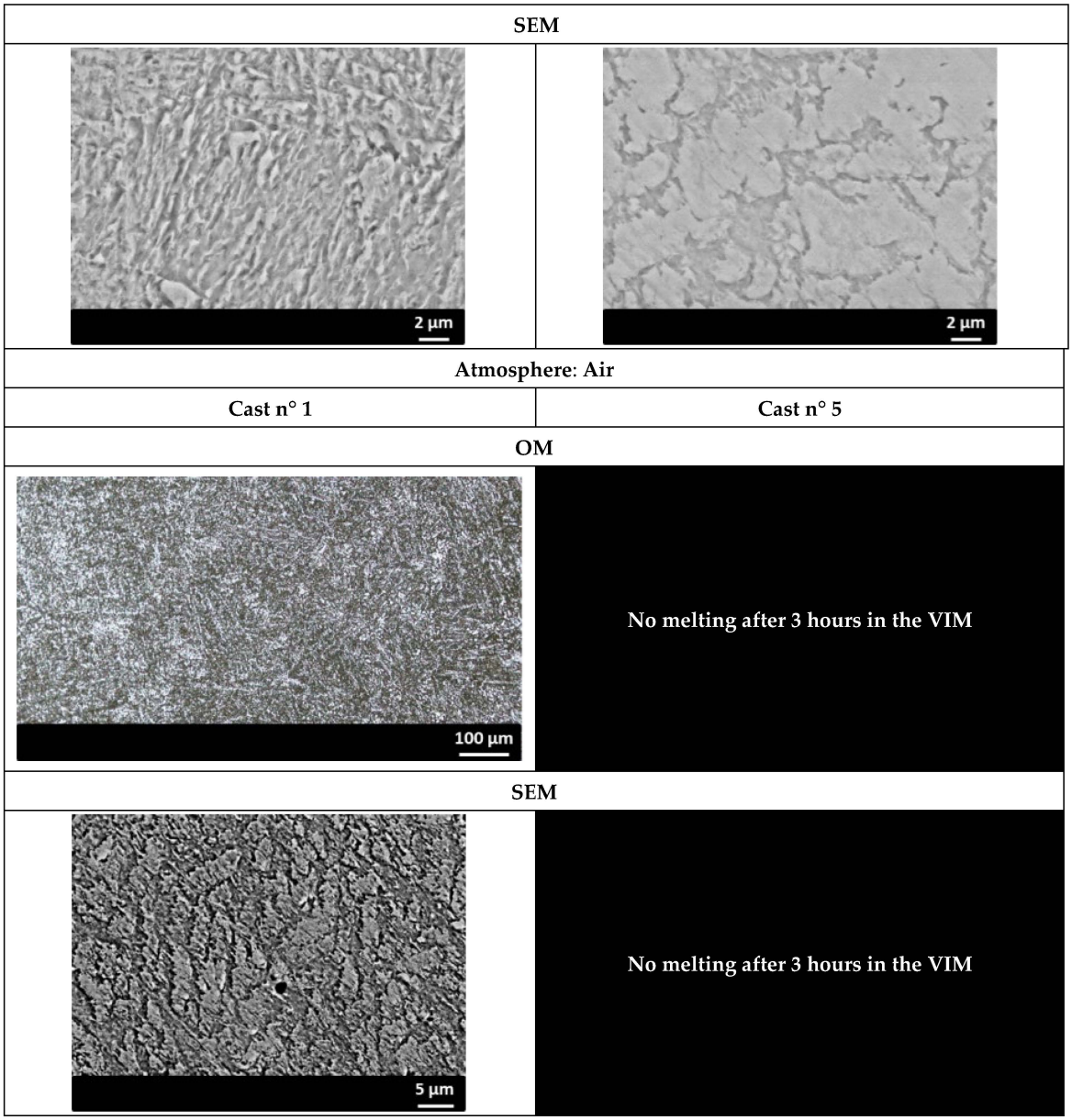

Figure 7. OM and SEM images of freshly casted plates after melting/casting cycles n° 1 and n° 5.

3.4. Impact of the Heat Treatment on the Physical and Mechanical Properties of the Casted Steels

3.4.1. Heat Treatment of Homogenization

The heat treatment of homogenization aims to reorganize the steel matrix chemically through atom diffusion to obtain a homogeneous composition over all the sample volume [48]. Such thermal actions are usually conducted in the range of 1000 to 1300 °C [49]. Herein, the homogenization of each casted sample was performed at 1100 °C for 30 min. The plate casted (n° 5) under vacuum was then cut into two identical pieces prior to being homogenized. One piece was homogenized in a regular muffle furnace (under air), while the second one was thermally treated in the VIM (under vacuum). To obtain an optimal homogenization, the homogenized sample should be cooled down by following thermodynamics equilibrium conditions. Consequently, the slowest cooling rate should be applied, and to do so, the sample was kept inside the furnace until reaching back 30 °C. This corresponded to a cooling rate close to 0.02 °C.s^{-1}. In order to compare the gas phase composition and conditions set during this work, the chemical composition of each thermally treated plate was then determined as summarized in Table 6.

Table 6. Chemical composition of the plates casted (n° 5) under vacuum, argon, and air before and after the homogenization (Hom.) treatment performed for each sample at 1100 °C for 30 min followed by a furnace cooling, as well as after the normalization treatment performed for each sample at 900 °C for 30 min (air cooling, furnace cooling for induction). The Fe wt.% balanced each composition.

Sample	Furnace (Atmosphere)	Condition	Composition (wt.%)								
			C	Mn	Si	Cr	Ni	Mo	Cu	Nb	P
Vacuum Cast n° 5	Regular muffle (air)	Before Hom.	0.249	0.436	1.127	0.471	1.148	0.397	0.150	0.019	0.008
		After Hom.	0.221	0.524	0.925	0.461	1.029	0.355	0.158	0.017	0.007
		Normalization	0.223	0.512	0.934	0.464	1.005	0.357	0.151	0.019	0.007
	VIM (vacuum)	Before Hom.	0.249	0.436	1.127	0.471	1.148	0.397	0.150	0.019	0.008
		After Hom.	0.228	0.518	1.008	0.457	1.116	0.378	0.155	0.018	0.008
		Normalization	0.222	0.498	1.043	0.455	1.132	0.381	0.152	0.018	0.009
Argon Cast n° 5	Regular muffle (air)	Before Hom	0.230	0.426	0.908	0.468	1.062	0.375	0.150	0.018	0.007
		After Hom.	0.224	0.497	0.915	0.459	1.046	0.369	0.154	0.015	0.007
		Normalization	0.226	0.479	0.909	0.465	1.042	0.371	0.150	0.016	0.007
Air Cast n° 1	Regular muffle (air)	Before Hom	0.227	0.159	0.247	0.362	1.063	0.374	0.160	0.007	0.006
		After Hom.	0.216	0.171	0.256	0.355	1.072	0.371	0.165	0.006	0.007
		Normalization	0.223	0.165	0.255	0.357	1.069	0.371	0.163	0.007	0.007

As shown in Table 6, by looking at all data reported before and after homogenization, whatever the condition and furnace used, the chemical composition of the tested steel remained quite constant after this thermal treatment. Moreover, as already observed with the homogenization of the as-received sample, the carbon content reached an expected value (see Tables 1, 2, 4 and 6), while the Mn content remained constant after the last melting/casting cycle. Such a result indicates that melting the sample allowed the diffusion of the segregated carbon while preventing it from the segregation through the casting. It is from notable differences between the two furnaces used that the presence of O_2 (air) induced the oxidation of elements with a high affinity with oxygen, as expected by following the Ellingham diagram [42].

The evolution of the reached microstructures when applying the homogenization heat treatment on each plate under the different conditions set herein was then depicted using optical and electronical microscopies, and the resulting clichés are reported in Figure 8. Since the chemical compositions (Table 6) were close for the plates casted under vacuum and argon, the obtained microstructures were typical and corresponded to a mix of ferrite and pearlite with proportions of approximately 30% and 70%, respectively. These stable phases (equilibrium) can be easily attributed, with the clear zone for ferrite and the darker zone for pearlite [50], and they are expected based on the slow cooling applied after the heat treatment of homogenization (i.e., 0.02 °C.s^{-1}).

However, when the homogenization heat treatment was conducted inside the induction furnace under vacuum, a more uniform distribution of phases was observed. As illustrated in Figure 8, the plate treated thermally in air also achieved a ferrite and pearlite microstructure; however, it exhibited a higher fraction of ferrite (50%) due to the loss of certain elements that stabilize austenite (such as Mn and Cr). This loss aligned with the observed compositional changes in this specific steel plate under different heat treatments (see Tables 1, 4 and 6). These findings highlight the critical role of the atmosphere during thermal treatments, as a vacuum environment not only preserves the chemical composition but also enhances the microstructural homogeneity. After obtaining a homogenized sample, a subsequent normalization thermal treatment should be performed to refine the grain size and achieve the targeted mechanical properties.

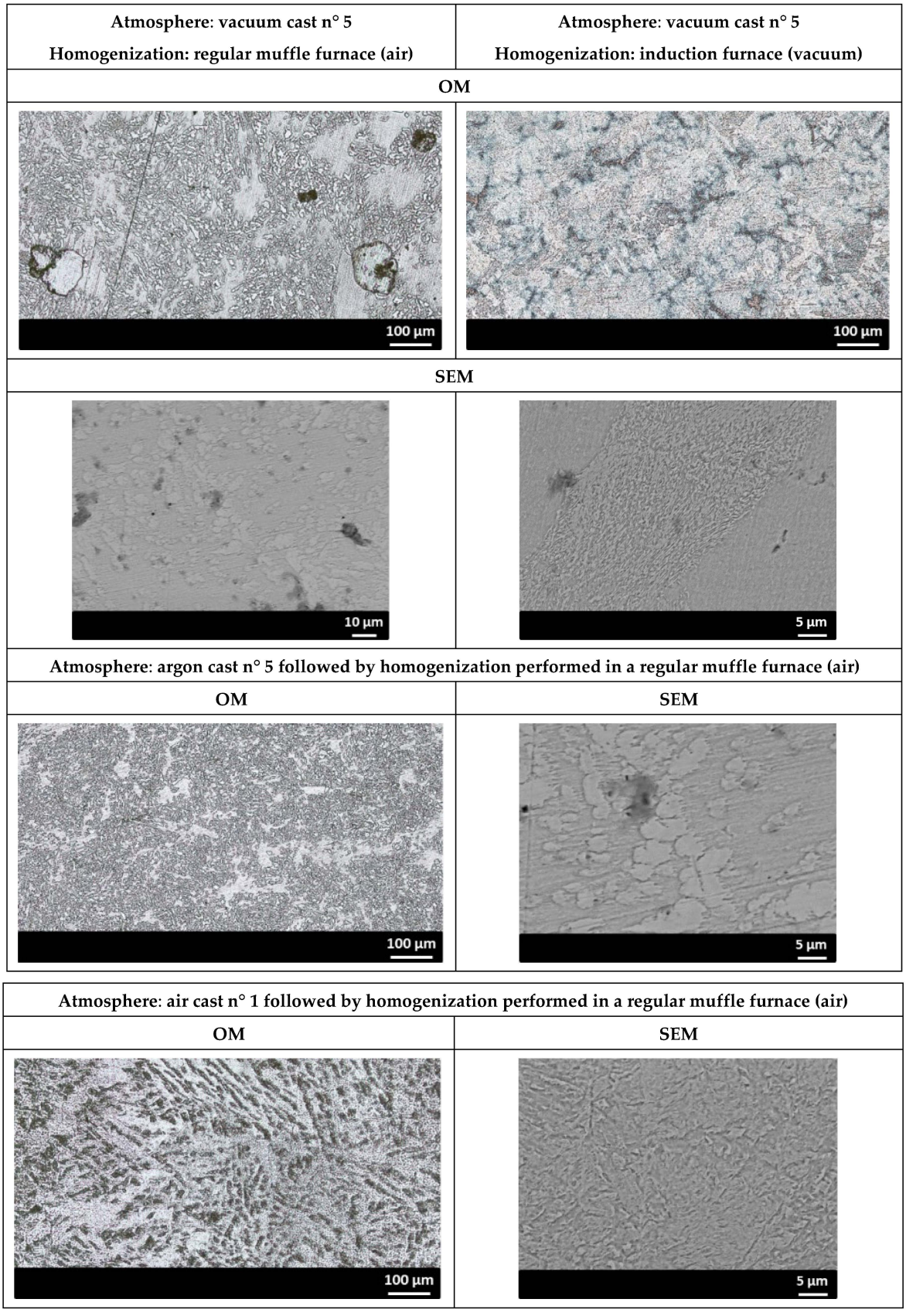

Figure 8. OM and SEM images of the homogenized plates for heat treatments realized inside a regular muffle (casted under vacuum, argon, and air) or inside an induction (casted under vacuum) furnace.

3.4.2. Heat Treatment of Normalization

The most common thermal treatment following homogenization is normalization [51]. Followed by a slow cooling, e.g., inside the furnace or under air, this thermal treatment aims to homogenize the grain size distribution. It consists of reaching a full austenitization and aims to prepare the steel to reach its final microstructure regarding the associated cooling, such as quenching in oil or water, ensuring the obtention of non-equilibrium phases such as bainite or martensite. Based on Equation (1), Ac_3 temperature was evaluated as close as 845 °C. Thus, each heat treatment of normalization was performed at 900 °C for 30 min, followed by three different cooling conditions performed: (*i*) inside the furnace (denoted FQ, 0.02 °C.s^{-1}), (*ii*) under air (denoted AQ, 30–50 °C.s^{-1}), and (*iii*) in water (denoted WQ, 100 °C.s^{-1}). Once more, the sample casted under vacuum (n° 5) was normalized in a regular muffle furnace or in an induction furnace to highlight the impact of the atmosphere on the normalization process with chemical composition, as depicted in Table 6. Regarding these different cooling methods, the resulting microstructures (observed by OM and SEM) are presented in Figure 9, while the associated hardness data collected for all tested conditions are summarized in Table 7.

The normalization made in the two types of furnaces led to a mix of ferrite and bainite (fractions of about 40% and 60%, respectively), as expected from the chemical composition (Table 6) and from the equilibrium phase diagram when a slow cooling is then applied (FQ conditions). In this case, the main difference lies in the grain size and the homogeneity of the obtain microstructure, which were impacted by the atmosphere conditions applied during the thermal treatment. Inert conditions (VIM furnace under vacuum) led to a grain size average of (6 $\pm$ 0.5) µm, indicating the presence of small grain size with an excellent homogeneity, while a much larger calculated average close to (10 $\pm$ 2.5) µm was observed when using air conditions inside a muffle furnace. In other words, small grains with the tiniest distribution were obtained when using a well-controlled atmosphere furnace when applying a given heat treatment. Moreover, one can notice that the inert atmosphere prevented carbide precipitation, as well as the decarburization phenomenon.

Then, by looking solely at data obtained when applying all thermal treatments inside the regular muffle furnace, one can note that all the samples casted under vacuum or argon exhibited similar microstructures.

For slow and intermediate cooling rates (e.g., FQ and AQ), due to nearly identical composition of the tested plates (see Table 6), the obtained microstructure consisted of ferrite and pearlite microstructures with a very low fraction of pearlite. Furthermore, the use of water quenching (WQ) led to the transformation of the austenite into metastable phases that seemed to be bainite. Regarding the casting made under air, leading to a loss of elements aiming at austenite stabilization, the microstructure analysis of the tested plate revealed that the ferrite became the most stabilized and consequently the main phase obtained when applying instead a slow (FQ) or an intermediate cooling rate (AQ). A pearlitic microstructure, in a lower amount, was also obtained by rapidly cooling the steel plate in water (WQ). This could be expected by looking at the chemical composition of this particular steel grade, highlighting the importance of reporting the chemical composition and the microstructure of the investigated steel before and after each steelmaking step and process. Such a result clearly revealed the critical importance of verifying the chemical composition before and after each thermal step (casting, homogenization, normalization, quenching, and tempering) and to report experimental conditions with great care. In fact, the targeted microstructures are the perfect combination between the chemical composition and the associated heat treatment conditions applied. The loss of a crucial element, such as the manganese used to improve the hardenability of the material, thus induces major changes on expected microstructures. Therefore, knowing the chemical composition before thermally treating a sample, e.g., after the previous thermal action, is crucial to anticipate the expected results and/or the feasibility of the heat treatment that should be performed.

Table 7. Effects of furnace type and experimental conditions on the microstructures and hardness of tested samples after their normalization performed at 900 °C for 30 min followed by a subsequent cooling performed inside the furnace (FQ), under air (AQ) or in water (WQ).

Sample	Furnace Used During the Normalization (Atmosphere)	Cooling Rate	Microstructure	Hardness (HB)
Vacuum cast n° 5 Homogenized (vacuum)	Induction (vacuum)	FQ	F + B	240
Vacuum cast n° 5 Homogenized (air)	Regular muffle (air)	FQ	F + P	203
	Regular muffle (air)	AQ	F + P	208
	Regular muffle (air)	WQ	B + M	467
Argon cast n° 5 Homogenized (air)	Regular muffle (air))	FQ	F + P	199
	Regular muffle (air)	AQ	F + B	223
	Regular muffle (air)	WQ	B + M	445
Air cast n° 1 Homogenized (air)	Regular muffle (air)	FQ	F	160
	Regular muffle (air)	AQ	F	163
	Regular muffle (air)	WQ	F + B	229

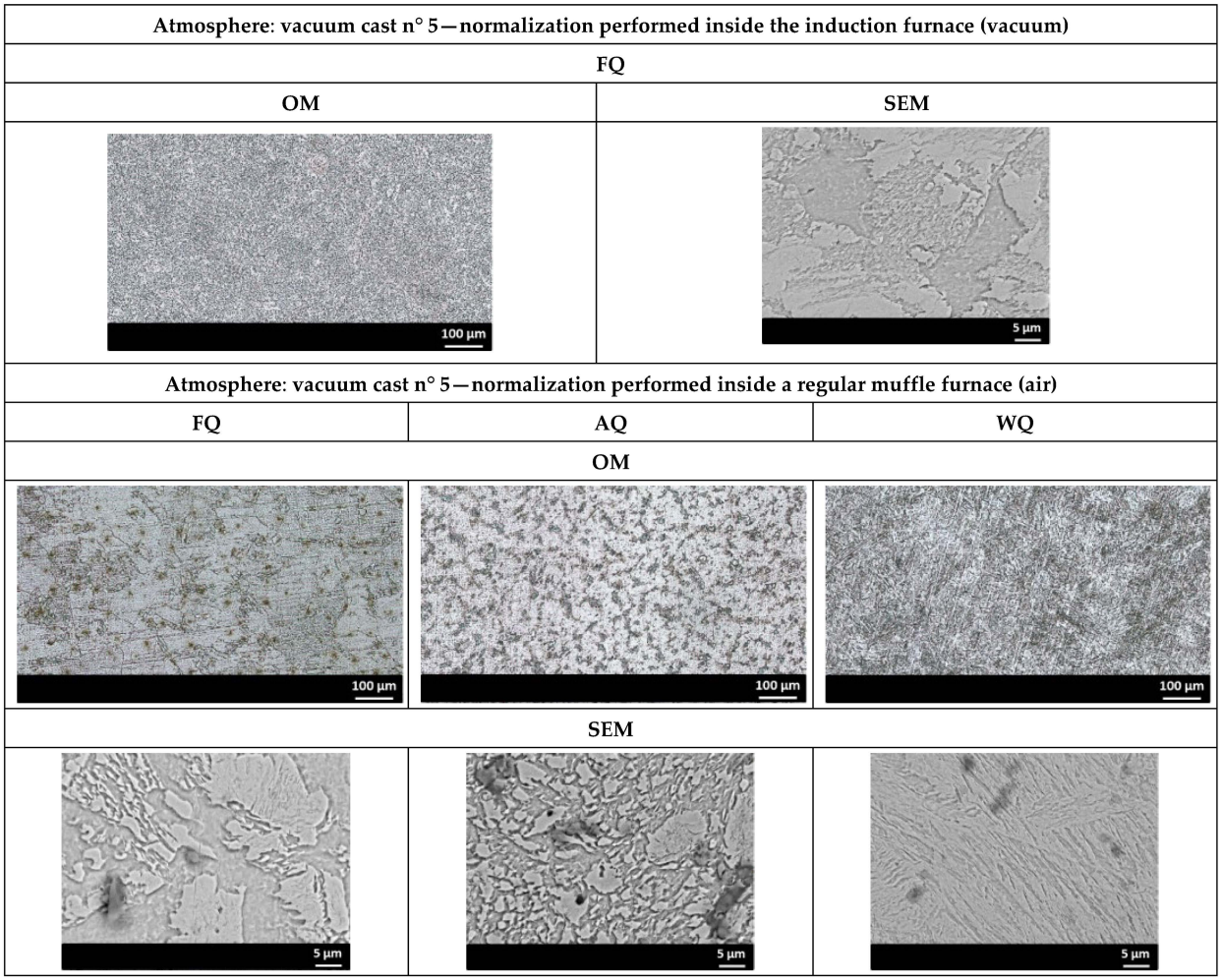

Figure 9. *Cont.*

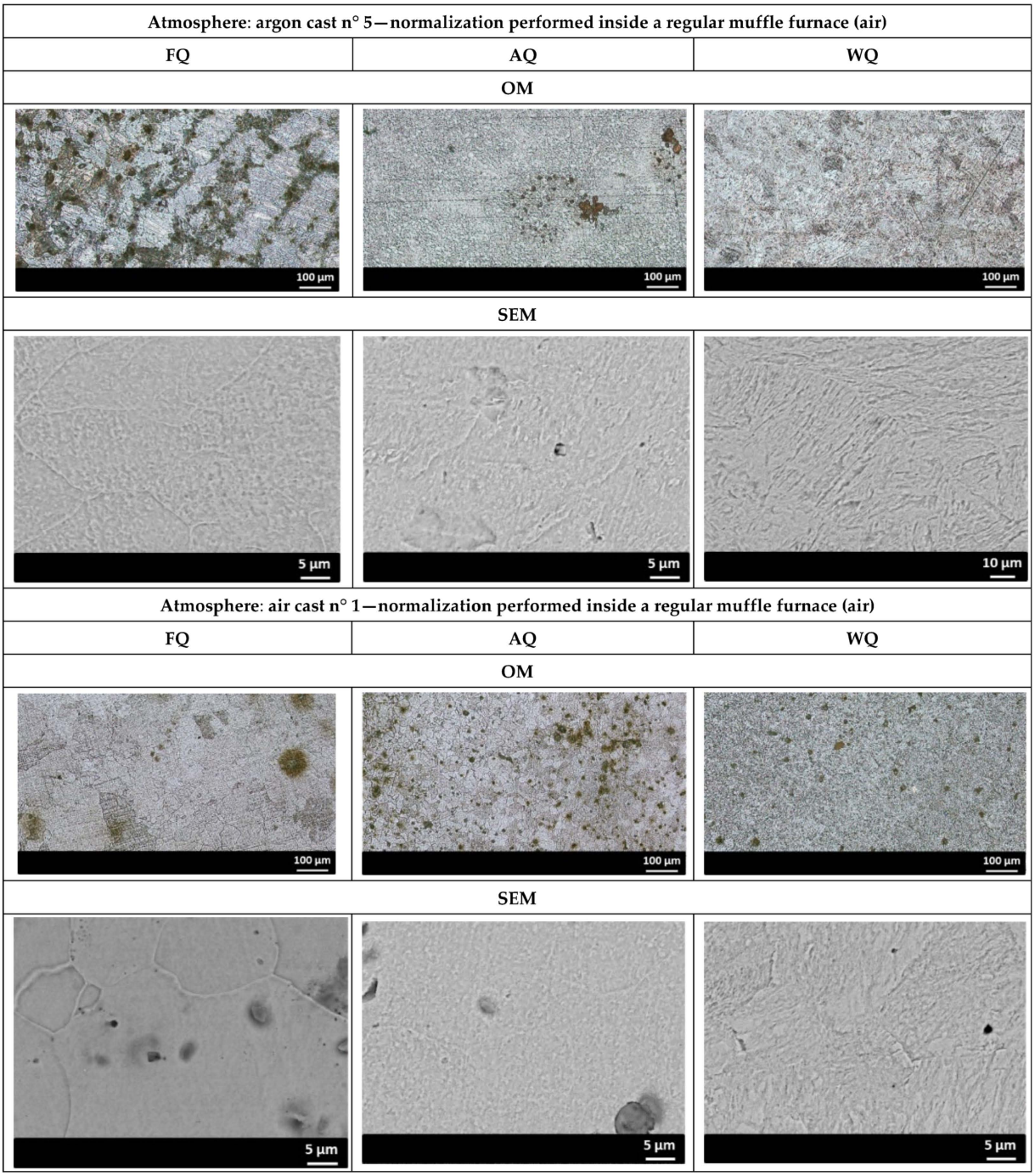

Figure 9. OM and SEM clichés observed for the normalized plates for heat treatments realized inside a regular muffle (casted under vacuum, argon, or air) or inside an induction (casted under vacuum) furnace prior to being cooled inside the furnace (FQ), or under air (AQ), or quenched in water (WQ).

Regarding hardness measurements, as summarized in Table 7 with the associated heat treatment conditions and the resulted microstructure, one can see the agreement between the measured hardness and the identified microstructures. In fact, harness values (*i*) lower than 200 HB were observed mainly for ferritic samples (i.e., those typically casted under air), (*ii*) close to 220 HB were observed for ferrite–bainite microstructures (higher for smaller grains), and (*iii*) higher than 450 HB were observed for bainitic–martensitic microstructures. This latest hardness confirms that the quenched samples were not fully martensitic as the measured harness values were much lower than those expected from a martensitic hardness, which is close to 500—600 HB.

This study clearly demonstrates that cooling rate, atmosphere, and chemical composition significantly influence the resulting microstructures and, consequently, the mechanical properties of the steel. This was validated through dilatometry measurements, as shown in Figures S4–S7 of the ESI, which highlight different phase change start temperatures depending on the cooling rate applied. For instance, phase changes were observed at 663 °C, 568 °C, 460 °C, and 385 °C for cooling rates of 0.02 °C.s^{-1}, 0.1 °C.s^{-1}, 1 °C.s^{-1}, and 10 °C.s^{-1}, respectively. The evolution of microstructures was also analyzed across all tested samples, with results displayed in Figures S8–S10 of the ESI. At the lowest cooling rate (0.02 °C.s^{-1}), the microstructure consisted of ferrite and pearlite, while at 0.1 °C.s^{-1}, bainite and pearlite phases appeared alongside some ferritic grains. At the highest cooling rate (1 °C.s^{-1}), a clear martensitic–bainitic microstructure was observed.

3.5. The Importance of Controlled Atmospheres for Scrap Recycling

The research involving PROTAC 500® underscores the importance of controlled atmospheres in pursuing sustainable, green steel production from scrap metals. Additional studies on three low-alloyed steel grades, detailed in the Case Studies Section of the ESI, support these findings. In case studies 1 and 2, two industrial low-alloyed steels (e.g., C40 and J2R samples) were firstly analyzed in terms of their chemical composition and microstructures in their as-received state. Selected scrap samples were then melted and cast in the VIM furnace under vacuum. Homogenization and normalization heat treatments, along with each cooling step, were performed under similar conditions as those applied to PROTAC 500® (see Figure 1) under vacuum inside the VIM. As shown in the Case studies Section of the ESI, in each case, the recycled steel exhibited chemical composition, phases, and microstructures comparable to the as-received material. This conclusion further emphasizes the importance of using an inert atmosphere not only during the melting and casting process but also throughout the subsequent heating and cooling treatments.

In the case of study 3, two scrap metals were analyzed, then melted and cast together in the VIM furnace under vacuum, following PROTAC 500® conditions. After subsequent thermal treatments and cooling (see Figure 1) performed inside the VIM furnace under vacuum condition, mass conservation was maintained across all analyzed elements (see ESI), confirming that the chemical composition of the as-produced low-alloyed steel can be reliably designed using a simple mass balance approach within the prior knowledge of each scrap's composition and mass. Very interestingly, in such a case, the VIM furnace could be used as a ladle furnace (LF) by using its addition chamber under controlled atmosphere to optimize the element addition during the secondary metallurgy step. In other words, by using a controlled atmosphere during both the melt/casting and thermal treatment processes, the recyclability of scrap metals can be maximized while achieving high-quality material properties, contributing to more efficient and environmentally friendly steelmaking practices.

These findings underscore the critical importance of considering the atmosphere during not only the melting/casting but also during heat treatments when recycling scrap steel to produce "green steel". Relying solely on time–temperature–transformation (TTT) and temperature-retained cooling (TRC) diagrams may be insufficient, as the atmosphere can significantly affect the outcome. In inert atmospheres, such as argon or vacuum, oxidation is prevented, maintaining the purity of the phases and ensuring the steel achieves its desired properties. Conversely, in oxidizing atmospheres, contamination from oxidation reactions can alter the steel's chemical composition and microstructure, leading to undesirable mechanical properties. To adhere to good research practices, scientists should provide the chemical composition of the steel grade before and after each heat-related process, which is unfortunately not the case in many studies.

4. Conclusions

This study, conducted using a non-conform commercial steel grade PROTAC 500®, emphasizes the importance of scrap recycling in steelmaking, particularly in relation to the

control of atmosphere composition during the melting and casting cycles in an induction furnace. The research focused on the chemical stability of the steel and its recyclability, demonstrating how successive melting/casting cycles affect the retention of elements in the material. It was shown that inert conditions, such as vacuum or argon, are ideal for maintaining the chemical composition during recycling. However, applied conditions also offer the potential to selectively remove certain elements, providing a controlled method for refining the composition of recycled steel. This highlights the induction furnace's significant capability to produce specific steel grades from scrap materials, enhancing its role in sustainable metallurgy and on the development of green steel strategies. This finding was also supported by the melting/casting cycle of three other low-alloyed steel grades.

Moreover, the study underscores the necessity of controlling the atmosphere during thermal treatments, such as homogenization and normalization, to ensure uniform chemical composition and grain size, both of which are critical for the material's mechanical properties. The VIM furnace, initially designed for melting scrap steels, proved effective as a heat treatment furnace as well. Treating steel samples under vacuum not only reduced grain size and narrowed grain distribution but also eliminated the decarburization or segregation issues commonly encountered in conventional air-based treatments.

The last part of the study reinforces the importance of conducting heat treatments in a controlled, step-by-step manner, with careful attention to parameters such as initial and final chemical composition, temperature, holding time, atmosphere, and cooling rate. This aligns with the principles of using equilibrium and non-equilibrium phase diagrams to precisely set up a cooling rate to be applied to a given chemical composition of a specific steel grade, which helps in predicting its final microstructure and mechanical properties.

All findings reported in this work highlight the potential of recycling scrap metals while achieving high-quality, targeted material properties through precise control of melting, casting, and heat treatment processes.

Supplementary Materials: The following supporting information can be downloaded at https://www.mdpi.com/article/10.3390/met14121317/s1. Figure S1: S1 Minilab 150 from GNR standard certificate. Figure S2: Hardness standard certificate. Figure S3: Dilatometry heating/cooling curve. Figures S4–S7: Dilatometry cooling profiles at 0.02 °C/s, 0.1 °C/s, 1 °C/S, and 10 °C/s, respectively. Figures S8–S10: The observed microstructures after dilatometry tests at cooling rates of 0.02 °C/s, 0.1 °C/s, and 1 °C/s, respectively. Table S1: List of equipment used in the present work. Table S2: Surface chemical composition (in weight wt.%) and hardness of the standard (low-alloyed steel), the as-received steel. The Case Studies section provides the data obtained for three other steel grades, which were produced using the same methodology and green steel strategy.

Author Contributions: Conceptualization, J.J.; methodology, B.B. and J.J.; validation, G.A.-l., A.B., B.B., Y.S., S.B.S. and J.J.; formal analysis, G.A.-l., A.B., B.B., Y.S. and J.J.; investigation, G.A.-l., A.B., B.B., Y.S., S.B.S. and J.J.; resources, J.A., S.B.S. and J.J.; data curation, A.B., S.B.S. and J.J.; writing—original draft, G.A.-l., B.B., Y.S. and J.J.; writing—review and editing, G.A.-l., A.B., B.B., Y.S., J.A., S.B.S. and J.J.; visualization, J.A. and J.J.; supervision, B.B. and J.J.; project administration, J.J.; funding acquisition, J.A. and J.J. All authors have read and agreed to the published version of the manuscript.

Funding: This research is jointly supported by the Mohammed VI Polytechnic University (UM6P) and by Maghreb Steel (grant number ARC-metallurgy AS-001).

Data Availability Statement: The original contributions presented in the study are included in the article/Supplementary Materials, further inquiries can be directed to the corresponding author.

Acknowledgments: The authors would like to acknowledge all administrative and technical support received from both Maghreb Steel and the UM6P ecosystems associated with the creation of the ARC-metallurgy Laboratory. In addition, the authors would like to acknowledge the SIJ Acroni company for supplying the benchmark material used during these experiments.

Conflicts of Interest: Author Sanae Baki Senhaji was employed by the company Maghreb Steel, Accelerated Research Center for Metallurgy (ARC Metallurgy–Maghreb Steel Site). The remaining authors declare that the research was conducted in the absence of any commercial or financial relationships that could be construed as a potential conflict of interest. Besides, the authors declare

that this study received funding from Maghreb Steel. The funder was not involved in the study design, collection, analysis, interpretation of data, the writing of this article or the decision to submit it for publication.

References

1. Tandon, V.; Thombre, M.A.; Patil, A.P.; Taiwade, R.V.; Vashishtha, H. Effect of Heat Input on the Microstructural, Mechanical, and Corrosion Properties of Dissimilar Weldment of Conventional Austenitic Stainless Steel and Low-Nickel Stainless Steel. *Metallogr. Microstruct. Anal.* **2020**, *9*, 668–677. [CrossRef]
2. El-Bagoury, N.; Moussa, M.E.; Ibrahim, K.; Ghayad, I.; Halfa, H. Influence of Cr and Solution Treatment on Structure and Properties of New Class Lightweight Fe–Mn–Al–C Stainless Steels. *Metallogr. Microstruct. Anal.* **2022**, *11*, 38–58. [CrossRef]
3. Pacheco, J.T.; de Oliveira, A.S.C.M. Additive Manufacturing of Duplex Stainless Steels: Assessment of Deposition Processes, Microstructure, and Properties. *Int. J. Adv. Manuf. Technol.* **2023**, *127*, 5013–5030. [CrossRef]
4. Qiao, Y.-X.; Zheng, Z.-B.; Yang, H.-K.; Long, J.; Han, P.-X. Recent Progress in Microstructural Evolution, Mechanical and Corrosion Properties of Medium-Mn Steel. *J. Iron Steel Res. Int.* **2023**, *30*, 1463–1476. [CrossRef]
5. Nasiri, Z.; Ghaemifar, S.; Naghizadeh, M.; Mirzadeh, H. Thermal Mechanisms of Grain Refinement in Steels: A Review. *Met. Mater. Int.* **2021**, *27*, 2078–2094. [CrossRef]
6. Jorge, J.C.F.; Souza, L.F.G.D.; Mendes, M.C.; Bott, I.S.; Araújo, L.S.; Santos, V.R.D.; Rebello, J.M.A.; Evans, G.M. Microstructure Characterization and its Relationship with Impact Toughness of C-Mn and High Strength Low Alloy Steel Weld Metals—A Review. *J. Mater. Res. Technol.* **2021**, *10*, 471–501. [CrossRef]
7. Cheng, H.; Luo, X.; Wu, X. Recent Research Progress on Additive Manufacturing of High-Strength Low-Alloy Steels: Focusing on the Processing Parameters, Microstructures and Properties. *Mater. Today Commun.* **2023**, *36*, 106616. [CrossRef]
8. Yin, R.-Y. Review on the Study of Metallurgical Process Engineering. *Int. J. Miner. Metall. Mater.* **2021**, *28*, 1253–1263. [CrossRef]
9. Wang, Z.; Bao, Y. Development and Prospects of Molten Steel Deoxidation in Steelmaking Process. *Int. J. Miner. Metall. Mater.* **2024**, *31*, 18–32. [CrossRef]
10. Xin, Z.; Zhang, J.; Peng, K.; Zhang, J.; Zhang, C.; Liu, Q. Modeling of LF Refining Process: A Review. *J. Iron Steel Res. Int.* **2024**, *31*, 289–317. [CrossRef]
11. Nian, Y.; Zhang, L.; Zhang, C.; Ali, N.; Chu, J.; Li, J.; Liu, X. Application Status and Development Trend of Continuous Casting Reduction Technology: A Review. *Processes* **2022**, *10*, 2669. [CrossRef]
12. Prifti, J.; Castro, M.; Squillacioti, R.; Cellitti, R. *Improved Rolled Homogeneous Armor (IRHA) Steel Through Higher Hardness*; United States Army Research Laboratory: Adelphi, MD, USA, 1997. Available online: https://apps.dtic.mil/sti/citations/ADA329222 (accessed on 21 July 2024).
13. Jena, P.K.; Mishra, B.; RameshBabu, M.; Babu, A.; Singh, A.K.; SivaKumar, K.; Bhat, T.B. Effect of Heat Treatment on Mechanical and Ballistic Properties of a High Strength Armour Steel. *Int. J. Impact Eng.* **2010**, *37*, 242–249. [CrossRef]
14. El-Bitar, T.; El-Shenawy, E.; El-Meligy, M.; Almosilhy, A.; Dawood, N. Development of Armor High Strength Steel (HSS) Mar-tensitic Plates for Troops Carriers. *Mater. Sci. Forum* **2016**, *879*, 489–494. [CrossRef]
15. Paristiawan, P.A.; Adjiantoro, B. Effect of Hardening and Tempering on Mechanical Properties and Microstructures of Armoured Laterite Steel in Various Quench Media. *AIP Conf. Proc.* **2021**, *2382*, 070002. [CrossRef]
16. Haiko, O.; Kaijalainen, A.; Pallaspuro, S.; Hannula, J.; Porter, D.; Liimatainen, T.; Kömi, J. The Effect of Tempering on the Mi-crostructure and Mechanical Properties of a Novel 0.4C Press-Hardening Steel. *Appl. Sci.* **2019**, *9*, 4231. [CrossRef]
17. Alibeyki, M.; Mirzadeh, H.; Najafi, M. Fine-Grained Dual Phase Steel via Intercritical Annealing of Cold-Rolled Martensite. *Vacuum* **2018**, *155*, 147–152. [CrossRef]
18. Das, D.; Chattopadhyay, P.P. Influence of Martensite Morphology on the Work-Hardening Behavior of High Strength Fer-rite-Martensite Dual-Phase Steel. *J. Mater. Sci.* **2009**, *44*, 2957–2965. [CrossRef]
19. Soleimani, M.; Mirzadeh, H.; Dehghanian, C. Processing Route Effects on the Mechanical and Corrosion Properties of Dual Phase Steel. *Met. Mater. Int.* **2020**, *26*, 882–890. [CrossRef]
20. Balbi, M.; Alvarez-Armas, I.; Armas, A. Effect of Holding Time at an Intercritical Temperature on the Microstructure and Tensile Properties of a Ferrite-Martensite Dual Phase Steel. *Mater. Sci. Eng. A* **2018**, *733*, 1–8. [CrossRef]
21. Bupesh Raja, V.K.; Palanikumar, K.; Rohith Renish, R.; Ganesh Babu, A.N.; Varma, J.; Gopal, P. Corrosion Resistance of Corten Steel—A Review. *Mater. Today Proc.* **2021**, *46*, 3572–3577. [CrossRef]
22. Mejía Gómez, J.A.; Antonissen, J.; Palacio, C.A.; De Grave, E. Effects of Si as Alloying Element on Corrosion Resistance of Weathering Steel. *Corros. Sci.* **2012**, *59*, 198–203. [CrossRef]
23. Chen, Z.; Yu, Q.; Zhao, L.; Zhang, C.; Gu, M.; Wang, Q.; Wang, G. Insight into the Role of Si on Corrosion Resistance of Weathering Steel in a Simulated Industrial Atmosphere. *J. Mater. Res. Technol.* **2023**, *26*, 487–503. [CrossRef]
24. Cano, H.; Díaz, I.; de la Fuente, D.; Chico, B.; Morcillo, M. Effect of Cu, Cr and Ni Alloying Elements on Mechanical Properties and Atmospheric Corrosion Resistance of Weathering Steels in Marine Atmospheres of Different Aggressivities. *Mater. Corros.* **2018**, *69*, 8–19. [CrossRef]
25. Farrugia, D.; Brown, S.; Lavery, N.P.; Pleydell-Pearce, C.; Davis, C. Rapid Alloy Prototyping for a Range of Strip Related Advanced Steel Grades. *Procedia Manuf.* **2020**, *50*, 784–790. [CrossRef]

26. Schrama, F.N.H.; Beunder, E.M.; Van den Berg, B.; Yang, Y.; Boom, R. Sulphur Removal in Ironmaking and Oxygen Steelmaking. *Ironmak. Steelmak.* **2017**, *44*, 333–343. [CrossRef]
27. Alves, P.C.; da Rocha, V.C.; Pereira, J.A.M.; Bielefeldt, W.V.; Vilela, A.C.F. Review and Planning of Experiments with Steel and Slag in Laboratory Furnace. *J. Mater. Res. Technol.* **2018**, *7*, 387–394. [CrossRef]
28. Kukartsev, V.A.; Kukartsev, V.V.; Tynchenko, V.S. Cast Iron and Steel Smelting in Induction Crucible Furnaces of Industrial Frequency. *Solid State Phenom.* **2020**, *299*, 530–534. [CrossRef]
29. Gertsyk, S.I.; Mineev, Y.A. Technology of Melting of a 12Kh18N10T Alloy in Induction Furnaces. *Russ. Metall.* **2021**, *2021*, 1645–1649. [CrossRef]
30. Serov, G.V.; Komissarov, A.A.; Tikhonov, S.M.; Sidorova, E.P.; Kushnerev, V.; Mishnev, P.A.; Kuznetsov, D.V. Effect of Deoxidation on Low-Alloy Steel Nonmetallic Inclusion Composition. *Refract. Ind. Ceram.* **2019**, *59*, 573–578. [CrossRef]
31. Osei, R.; Lekakh, S.; O'Malley, R. Effect of Cu Additions on Scale Structure and Descaling Efficiency of Low C Steel Reheated in a Combustion Gas Atmosphere. *Oxid. Met.* **2022**, *98*, 363–383. [CrossRef]
32. Cabrilo, A.; Geric, K. Weldability of High Hardness Armor Steel. *Adv. Mater. Res.* **2016**, *1138*, 79–84. [CrossRef]
33. Savic, B.; Cabrilo, A. Effect of Heat Input on the Ballistic Performance of Armor Steel Weldments. *Materials* **2021**, *14*, 3617. [CrossRef] [PubMed]
34. Sabzi, M.; Farzam, M. Hadfield Manganese Austenitic Steel: A Review of Manufacturing Processes and Properties. *Mater. Res. Express* **2019**, *6*, 1065c2. [CrossRef]
35. Mahlami, C.S.; Pan, X. An Overview on High Manganese Steel Casting. In Proceedings of the 71st World Foundry Congress: Advanced Sustainable Foundry, Bilbao, Spain, 19–21 May 2014.
36. Yang, D.; Xiong, Z.; Zhang, C.; Feng, G.; Cheng, Z.; Cheng, X. Evolution of Microstructures and Mechanical Properties with Tempering Temperature of a Pearlitic Quenched and Tempered Steel. *J. Iron Steel Res. Int.* **2022**, *29*, 1393–1403. [CrossRef]
37. Ludlow, V.; Normanton, A.; Anderson, A.; Thiele, M.; Ciriza, J.; Laraudogoitia, J.; van der Knoop, W. Strategy to Minimise Central Segregation in High Carbon Steel Grades during Billet Casting. *Ironmak. Steelmak.* **2005**, *32*, 68–74. [CrossRef]
38. Guo, F.; Wang, X.; Wang, J.; Misra, R.D.K.; Shang, C. The Significance of Central Segregation of Continuously Cast Billet on Banded Microstructure and Mechanical Properties of Section Steel. *Metals* **2020**, *10*, 76. [CrossRef]
39. Zhang, M.; Bao, Y.; Zhao, L.; Li, X. Improvement of Carbon Segregation in Cast Bloom and Heredity in Hot-Rolled Bar. *Metall. Res. Technol.* **2021**, *118*, 610. [CrossRef]
40. Choudhary, S.K.; Ganguly, S. Morphology and Segregation in Continuously Cast High Carbon Steel Billets. *ISIJ Int.* **2007**, *47*, 1759–1766. [CrossRef]
41. Trzaska, J. Calculation of Critical Temperatures by Empirical Formulae. *Arch. Metall. Mater.* **2016**, *61*, 981–986. [CrossRef]
42. Epifano, E.; Monceau, D. Ellingham Diagram: A New Look at an Old Tool. *Corros. Sci.* **2023**, *217*, 111113. [CrossRef]
43. Pioro, L.S.; Pioro, I.L. Reprocessing of Metallurgical Slag into Materials for the Building Industry. *Waste Manag.* **2004**, *24*, 371–379. [CrossRef] [PubMed]
44. Kim, J.H.; Gu, G.; Kwon, M.-H.; Koo, M.; Kim, E.-Y.; Kim, J.-K.; Lee, J.S.; Suh, D.-W. Microstructure and Tensile Properties of Chemically Heterogeneous Steel Consisting of Martensite and Austenite. *Acta Mater.* **2022**, *223*, 117506. [CrossRef]
45. Wang, W.; Wei, P.; Liu, H.; Zhu, C.; Deng, G.; Liu, H. A Micromechanics-Based Machine Learning Model for Evaluating the Microstructure-Dependent Rolling Contact Fatigue Performance of a Martensitic Steel. *Int. J. Mech. Sci.* **2023**, *237*, 107784. [CrossRef]
46. Sun, C.; Fu, P.-X.; Ma, X.-P.; Liu, H.-H.; Du, N.-Y.; Cao, Y.-F.; Liu, H.-W.; Li, D.-Z. Effect of Matrix Carbon Content and Lath Martensite Microstructures on the Tempered Precipitates and Impact Toughness of a Medium-Carbon Low-Alloy Steel. *J. Mater. Res. Technol.* **2020**, *9*, 7701–7710. [CrossRef]
47. Badkoobeh, F.; Mostaan, H.; Rafiei, M.; Bakhsheshi-Rad, H.R.; Berto, F. Microstructural Characteristics and Strengthening Mechanisms of Ferritic–Martensitic Dual-Phase Steels: A Review. *Metals* **2022**, *12*, 101. [CrossRef]
48. Hofinger, M.; Staudacher, M.; Ognianov, M.; Turk, C.; Leitner, H.; Schnitzer, R. Microstructural Evolution of a Dual Hardening Steel during Heat Treatment. *Micron* **2019**, *120*, 48–56. [CrossRef]
49. Ravi, A.M.; Kumar, A.; Herbig, M.; Sietsma, J.; Santofimia, M.J. Impact of Austenite Grain Boundaries and Ferrite Nucleation on Bainite Formation in Steels. *Acta Mater.* **2020**, *188*, 424–434. [CrossRef]
50. Zhang, S.; Romo, S.; Giorjao, R.A.; Leao, P.B.P.; Ramirez, A.J. EBSD Analysis of Strain Distribution and Evolution in Ferritic-Pearlitic Steel under Cyclic Deformation at Intermediate Temperature. *Mater. Charact.* **2022**, *193*, 112293. [CrossRef]
51. Rohit Sai Krishna, A.; Vamshi Krishna, B.; Sashank, T.; Harshith, D.; Subbiah, R. Influence and Assessment of Mechanical Properties on Treated P91 Steel with Normalizing Processes. *Mater. Today Proc.* **2020**, *27*, 1555–1558. [CrossRef]

Disclaimer/Publisher's Note: The statements, opinions and data contained in all publications are solely those of the individual author(s) and contributor(s) and not of MDPI and/or the editor(s). MDPI and/or the editor(s) disclaim responsibility for any injury to people or property resulting from any ideas, methods, instructions or products referred to in the content.